The Impact of Aqueous Phase Replacement Reaction on the Phase State of Internally Mixed Organic/ammonium Aerosols

Hui Yang, Fengfeng Dong, Li Xia, Qishen Huang, Shufeng Pang, Yunhong Zhang

School of Chemistry and Chemical Engineering, Beijing Institute of Technology, Beijing, 100081, People's Republic of China

Correspondence: Qishen Huang (qishenh@bit.edu.cn), Shufeng Pang (sfpang@bit.edu.cn)

Abstract. Aerosol phase state is crucial for air quality, climate, and human health. Atmospheric secondary aerosols are often internally mixed with organic and inorganic components, particularly dicarboxylic acids, ammonium, sulfate, nitrate, and chloride. These complex compositions enable aqueous reaction between organic and inorganic species, significantly complicating aerosol phase behavior during aging and making phase predictions challenging. We investigated carboxylate/ammonium salt mixtures using in-situ infrared spectroscopy. The di- and tri- carboxylates included sodium pyruvate (SP), sodium tartrate (ST), and sodium citrate (SC), while the ammonium salts included NH_4NO_3, NH_4Cl, and $(NH_4)_2SO_4$. Our results demonstrated that aqueous replacement reactions between carboxylates and ammonium salts was promoted by the formation and depletion of NH_3 as relative humidity (RH) changed. Solid $NaNO_3$, SP, and Na_2SO_4 formed in SP/ammonium aerosol at 35.7%~12.7%, 64% and 65.5%~60.1% RH, respectively. In contrast, reactions between ST or SC and $(NH_4)_2SO_4$ was incomplete due to the gel structure of SC or ST at low RH. Upon hydration, the deliquescence RH of Na_2SO_4 in SP/$(NH_4)_2SO_4$ (88.8%-95.2%) and $NaNO_3$ in SP/NH_4NO_3 (76.5-81.9%) are higher than those of pure inorganic aerosols. Unexpectedly, aqueous Na_2SO_4 crystallized upon humidification in ST/$(NH_4)_2SO_4$ particles at 43.6% RH and then deliquesced with increasing RH. This is attributed to decreased viscosity and increased ion mobility, which overcome the kinetic inhibition of ion movement, leading to nucleation and growth of Na_2SO_4 crystal. Our findings highlight the intricate interplay between chemical components within organic/inorganic aerosol, the impact of replacement reactions on aerosol aging and phase state, and subsequently on atmospheric processes.

1 Introduction

The phase state of atmospheric aerosols (e.g., liquid, solid, highly viscous, or phase separated) is arguably one the most crucial properties which dictates air quality, the climate and human health via atmospheric chemical and

physical processes (e.g., chemical reactions, aerosol aging, regional transport, and cloud formation) (Freedman et

al., 2024). However, the complex aerosol composition and various reaction pathways, results in complicated

30   aerosol phase behavior that is hard to predict (Zhang et al. 2024). As ambient relative humidity (RH) changes, the

phase states of atmospheric aerosol particles can be altered by the uptake and loss of water (Koop et al., 2001),

consequently affecting light absorption and scattering (Nemesure et al., 1995; Pilinis et al., 1995), cloud

condensation nuclei (CCN) activity (Svenningsson et al., 1997; Lreidenweis et al., 2005), chemical diffusion in

aerosols, gas-particle partitioning (Shiraiwa et al., 2012), and heterogeneous reactions (Liu et al., 2016).

35   Understanding the phase behaviors and water content of atmospheric aerosols is therefore essential for elucidating

their impacts on global climate and tropospheric chemistry.

Atmospheric aerosols consist of various organic and inorganic species, with carboxylic acids/salts and

ammonium salts as one of the most abundant organic and inorganic components, respectively. While ambient RH

fluctuates, most inorganic aerosols undergo a transition between liquid and solid states (i.e., efflorescence and

40   deliquescence), whereas most organic aerosols exhibit gradual water uptake and loss, leading to residual water in

non-effloresced, quasi-liquid states (Prenni et al., 2003; Zardini et al., 2008) or amorphous quasi-solid states (Peng

et al., 2001; Marcolli et al.; Liu et al.; 2008). For multicomponent atmospheric organic/inorganic aerosols, due to

intermolecular interactions and reactions between organic and inorganic components, the response of the water

content and phase state of aerosol particles to the ambient RH becomes even more complex. Organics can decrease

45   the surface activity of particles due to hydrophobic carbon chains and hydrophilic head groups. Additionally,

viscous states owing to intermolecular interactions at low humidity can be formed, leading to limited water

absorption. Studies have investigated the phase transition of aerosol particles constitute of organic acids and

inorganic salts (Shi et al., 2012; Wang et al., 2017). The effect of organic acids on the phase state of inorganic

salts depends on chemical composition and organic mass fractions (Huang et al., 2022; Jing et al., 2016).

50   Atmospheric particles can serve as micro-reactors, with their physical and chemical properties playing

pivotal roles in determining reactivity, heterogeneous uptake, and the liberation of trace gases (Jia et al., 2021).

Recent studies have shown that replacement reaction between organics and inorganic salts, which produces weak

bases and acids, can be promoted in aqueous phase aerosols by gas evaporation or solid formation (Wang et al.,

2019; Yang et al., 2019; Chen et al., 2021). For example, Ma et al. (Ma et al., 2019) conducted a comprehensive

55   study on the hygroscopic behavior and chemical reaction of oxalic acid and nitrate mixed particles and validated

the impact of metal oxalate complex formation on aerosols hygroscopic growth. Their results can explain the field

observation for Ca and Zn oxalate complexes in Asian dust aerosols (Furukawa et al., 2011). Ma et al. (Ma et al.,

2022) reported the nitrate depletion and HNO$_3$ release in internally mixed NaNO$_3$ and dicarboxylic acid aerosols. The reaction, also a replacement reaction, depended upon the aerosol drying rate and the NaNO$_3$ phase state acted

60   as a key regulator for nitrate depletion, which further affected the HONO liberate (Li et al., 2024). Du et al. investigated the impact of pH and RH on the displacement of HNO$_3$ and NH$_3$ by malonic acid (Du et al., 2021) and sodium succinate (Du et al., 2020), and discovered that low humidity conditions both facilitated the volatilization of nitric acid, meanwhile an increase in acidity had an opposite effect for HNO$_3$ and NH$_3$ substitution reaction. Chen et al. elucidated the thermodynamics and kinetics of the replacement reactions using

65   the multiphase buffer theory and a diffusion-controlled mass-transfer function, respectively (Chen et al., 2022). However, due to the lack of information on the correlation between the crystallization process and humidity changes, which results in the uncertainty in aerosol phase state, the kinetic processes based on the model cannot be accurately taken aerosol phase state into account.

Aerosol composition, the reactivity of replacement reactions, and the phase state are intercorrelated

70   parameters. The inhomogeneity of aerosol components can significantly impact the degree of reactivity, which is associated with changes in aerosol phase state, can induce comprehensive phase states (i.e., the coexistence of solid and liquid, liquid-liquid phase separation, and solid in a viscous phase) (Zong et al., 2022). The crystallization accompanying chemical reactions is a multi-step process involving ion migration, formation of ion pairs, nucleation, and growth processes. Depending on the nature and molecular structure of individual

75   compounds, the degree of reaction, as well as the efflorescence relative humidity (ERH) and deliquescence relative humidity (DRH), can all vary. Therefore, exploring the impact of different organic and inorganic salts on reactivity, particularly the reactivity for replacement reactions, is significant for the prediction of aerosol phase states.

In this study, internally mixed particles composed of typical organic salts and ammonium salts were selected to investigate the replacement reactions and the impact on aerosol phase state. The organic acid salts used included

80   sodium tartrate, sodium citrate, and sodium pyruvate, which all contains carboxylates. The ammonium salts included ammonium nitrate, ammonium chloride, and ammonium sulfate. The effects of various ammonium compounds on reactivity and aerosol phase state, when mixed with the same organic acid salts, such as sodium pyruvate, were analyzed. Additionally, the physical properties dependent on the individual component ratio in particles were examined using the mixture of ammonium chloride and sodium pyruvate. While sodium pyruvate

85   exhibited clear efflorescence and deliquescence phenomena, sodium tartrate and sodium citrate formed a gel-like state at low humidity. The differences observed in reactions and phase transitions upon interaction with ammonium sulfate were thoroughly explored. This work contributes to a better understanding of the correlation

between chemical composition, replacement reaction, and aerosol phase state in organic-inorganic aerosols, thereby playing an essential role in improving the prediction of aerosol phases state and understanding climate
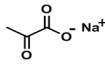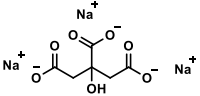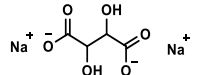
90   effects.

2 Materials and methods

2.1 Sample preparation

The 0.2 $mol \cdot L^{-1}$ mixture solutions of organic acid salts and ammonium salts were prepared using three distilled water. The organic acid salts include sodium pyruvate (SP), sodium citrate (SC), and sodium tartrate (ST). The

95   ammonium salts include $(NH_4)_2SO_4$, NH_4NO_3 and NH_4Cl. In a mixture system, one organic acid salt was mixed with one type of ammonium salts at various molar ratios (e.g., 2:1, 1:1, 2:3, and 1:2). The mixture solutions were aerosolized into aerosol droplets with an average diameter of 5μm. All compounds were used without further purification before experiment. The molecular structure and properties of the compounds involved in this study are listed in Table 1.

100

Table 1: The molecular structure of inorganic and organic compounds

Compound	Molecular structure	Dissociation constant of conjugate acid	Solubility in 100g H₂O (20°C)	Molecular weight (Da)
Ammonium nitrate	NH_4NO_3	**NA**	190g	80.043
Ammonium chloride	NH_4Cl	**NA**	37.2g	53.49
Ammonium sulfate	$(NH_4)_2SO_4$	**NA**	75.4g	132.14
Sodium pyruvate		$K_a = 3.2 \times 10^{-3}$	47g	82.03
Sodium citrate		$K_{a,1} = 7.4 \times 10^{-4}$ $K_{a,2} = 1.7 \times 10^{-5}$ $K_{a,3} = 4.0 \times 10^{-7}$	154g	258.07
Sodium tartrate		$K_{a,1} = 1.04 \times 10^{-3}$ $K_{a,2} = 4.55 \times 10^{-5}$	33.3g	194.05

2.2 ATR-FTIR measurement

The ATR-FTIR measurement was conducted using a FTIR spectrometer (Nicolet Magna-IR model 560) equipped

with a liquid-nitrogen-cooled mercury-cadmium-telluride (MCT) detector. A RH-controlling system, composed

of a high-purity water reservoir, mass flowmeter and vacuum bump, was connected to the FTIR spectrometer.

105 The RH was controlled by the mixing ratio of a wet nitrogen gas flow (saturated by water vapor), and a dry

nitrogen gas flow. The total flow rate of the two nitrogen gas flows was 500 mL min^{-1}, and the flow rate of the

wet and dry nitrogen gas flow were controlled by mass flow controllers. During the experiments, the RH was

monitored by humidity and temperature sensors coupled to a data logger at the outlet of the sample chamber. The

detailed instrumental information can be found in our study (Zhang et al., 2014). Prior to the ATR-FTIR

110 measurement, the RH was kept at the highest level in the sample chamber. The aerosols were atomized and

introduced into the sample chamber to be deposited onto the ZnSe substrate under the high RH condition. At room

temperature, the spectral resolution and the spectral range of the ATR-FTIR are 4 cm^{-1} and 800-4000 cm^{-1},

respectively.

2.3 Data processing

115 The IR spectra of aerosols were obtained by subtracting IR of water vapor at corresponding RH from raw IR

spectra without any smoothening. The water content at each RH level was gained by integrating the bands at 3360-

3690 cm^{-1} in the corresponding IR spectra. The relative water content was achieved by normalizing the peak area

of the water band (3360-3690 cm^{-1}) at a specific RH to that at the maximum RH.

3 Results and Discussion

120 **3.1 Spectral change and phase behavior of pure inorganic and organic aerosols**

The IR spectra of individual components, namely, ammonium nitrate, ammonium sulfate, ammonium chloride,

sodium pyruvate, sodium citrate, and sodium tartrate are shown in the Supporting Information (Fig. S1). The

features of the IR spectra can be used to differentiate the phase state of each compound. For example, for sodium

tartrate, the characteristic peaks of the aqueous phase and solid phase are located at 1069 cm^{-1} and 1055 cm^{-1},

125 respectively. Sodium citrate exhibits double sharp peaks at 1308 and 1278 cm^{-1} during crystallization. For pure

sodium pyruvate, the characteristic peaks of solid phase appear at 1405 cm^{-1}, and the band at 1176 cm^{-1} shifted to

1186 cm^{-1}. As for solid NH$_4$Cl, bands at 3130 and 1402 cm^{-1} are the characteristic IR peaks. When NH$_4$Cl was

mixed with sodium pyruvate, the band at 1402 cm^{-1} may overlap with the 1405 cm^{-1} and become indistinguishable;

therefore, the band at 3130 cm^{-1} was used as the feature for solid NH$_4$Cl, and the band 1186 cm^{-1} was applied to

130 characterize solid sodium pyruvate. For NH$_4$NO$_3$ and (NH$_4$)$_2$SO$_4$, when the phase transition from aqueous to solid

phase occurs, the NH_4^+ bands exhibit dissimilarity: shifting from 1448 cm^{-1} to 1417 cm^{-1} for NH_4NO_3, and from

1443 cm^{-1} to 1412 cm^{-1} for $(NH_4)_2SO_4$. When NH_4NO_3 and $(NH_4)_2SO_4$ are mixed with organic salts, the NH_4^+

bands can overlap with the characteristic peaks of sodium citrate and sodium tartrate in the same wavenumber

region, leading to difficulties in assigning the peaks to specific solid ammonium salts.

135 The IR spectra on dehydration and hygroscopic behavior of organics (sodium pyruvate, sodium citrate, and

sodium tartrate) during RH change were shown in Fig. S2. For pure organic compounds, the response of water

content in aerosols can be applied to elucidate phase transition. Sodium pyruvate aerosols effloresced at 63-60.5%

RH upon dehydration, corresponding to a sudden change in water content. In comparison, the water content of

pure sodium citrate and sodium tartrate aerosols decreased gradually upon dehumidification, indicating the

140 formation of a viscous state instead of solid phase (Mikhailov et al., 2009). The formation of viscous phase was

also consistent with the absence of solid features in IR spectra and the residual water peak at 3360 cm^{-1}. Upon

humidification, sudden water uptake occurred at 47.1-49.8% RH for sodium citrate, and at 55.7-59% RH for

sodium tartrate aerosols. Previous study has shown that similar abrupt water absorbance during humidification

was observed for viscous sucrose (Madawala et al., 2021) and $MgSO_4$ aerosols (Wang et al., 2018), which was

145 attributed to the hydration of aerosols during the phase transition from gel state to aqueous state. Hence, the abrupt

change in water content of the sodium citrate and sodium tartrate aerosols is due to the phase transition from a

viscous state to an aqueous state.

### 3.2 Spectral change and phase behavior of mixture organic/inorganic aerosols

Sodium pyruvate (SP) was mixed with various ammonium salts, including $(NH_4)_2SO_4$, NH_4Cl and NH_4NO_3. Fig.

150 1 illustrates their IR spectra as the RH decreased. The data for $SP/(NH_4)_2SO_4$ (Fig. 1(a)) have been reported by

Yang et al. (2019). The band at 3400 cm^{-1}, assigned to OH stretching mode of water, became weaker upon

dehydration, suggesting a gradual loss of liquid water content. Concurrently, the bands at 1708 cm^{-1} and 1355 cm^{-1}

gradually diminished, indicating a decrease in the quantity of SP in the aerosols phase. In the blue frame of Fig.

1(a), the enlarged IR feature of SP depicted the gradual weakening of 1176 cm^{-1} peak, which disappeared at 65.7%

155 RH, implying the complete SP depletion from the aerosols. The overlapping nature of the v_4-NH_4^+ mode, located

at ~1440 cm^{-1} in the aqueous phase or 1412 cm^{-1} in the solid phase, with the bands of SP at 1424 cm^{-1} or 1406 cm^{-1},

renders the determination of the phase state of $(NH_4)_2SO_4$ ambiguous. Accompanying the SP depletion, we

noted the appearance of a band at 1132 cm^{-1} at 65.7%, followed by its subsequent increase with further decreasing

RH. Tan et al investigated the efflorescence of Na_2SO_4, and assigned the 1132 cm^{-1} band to solid Na_2SO_4 (Tan et

160   al., 2014). In addition, the ν_1-SO_4^{2-} mode effectively discerns the sulfate phase state, with a peak at 980 cm^{-1} indicating the aqueous state and a peak at 996 cm^{-1} denoting the solid state (Miñambres et al., 2013). The purple frame of Fig. 1(a) showed the emergence of the 995 cm^{-1} band at 65.5% RH, accompanied by the diminishing 980 cm^{-1} band. At 60.1% RH, the 980 cm^{-1} disappeared, indicating the complete crystallization of Na_2SO_4.

For SP/NH_4Cl aerosols, the IR bands for SP at 1708 cm^{-1} 1355 cm^{-1} and 1627 cm^{-1} became weaker at lower

165   RH levels (Fig. 1(b)), indicating the decrease in SP content. As depicted in the blue frame of Fig. 1(b), both the solid IR band (1186 cm^{-1}) and the aqueous IR band of SP (1176 cm^{-1}) can be found at and below 23.7% RH, implying the coexistence of liquid and solid SP in SP/NH_4Cl aerosols. Additionally, the band at 1404 cm^{-1} became prominent at 23.7% RH. Given the comparable peak height between 1353 cm^{-1} and 1405 cm^{-1} in the IR spectrum of solid SP, the band at 1404 cm^{-1} likely originated from solid NH_4Cl, consistent with the sharp bands at 3130 and

170   3036 cm^{-1} (Max et al., 2013). According to previous studies, NaCl should form in the system, however, the formation of NaCl cannot be confirmed merely from the IR spectrum as NaCl exhibits no IR absorptions.

For SP/NH_4NO_3 particles, we observed similar SP loss, denoted by weaker SP band adsorption upon dehydration, along with a stronger band at 1355 cm^{-1}, an IR feature corresponding to the efflorescence of $NaNO_3$ (1352 cm^{-1} and 836 cm^{-1}) (Ren et al., 2016). When RH decreased to 35.7%, the band for solid $NaNO_3$ at 836 cm^{-1}

175   appeared (Fig. 1(c), purple frame), coexisting with the 829 cm^{-1} band for aqueous NO_3^-, indicating the presence of liquid NO_3^- across the RH range of 35.7%-32%. At 12.7% RH, only the band at 836 cm^{-1} was present, suggesting the crystallized $NaNO_3$ without liquid NO_3^- (Zhang et al., 2014). In the blue frame of Fig. 1(c), the band at 1176 cm^{-1} shifts slightly to 1180 cm^{-1} instead of the solid SP band at 1186 cm^{-1}, suggesting semi-solid SP rather than solid SP.
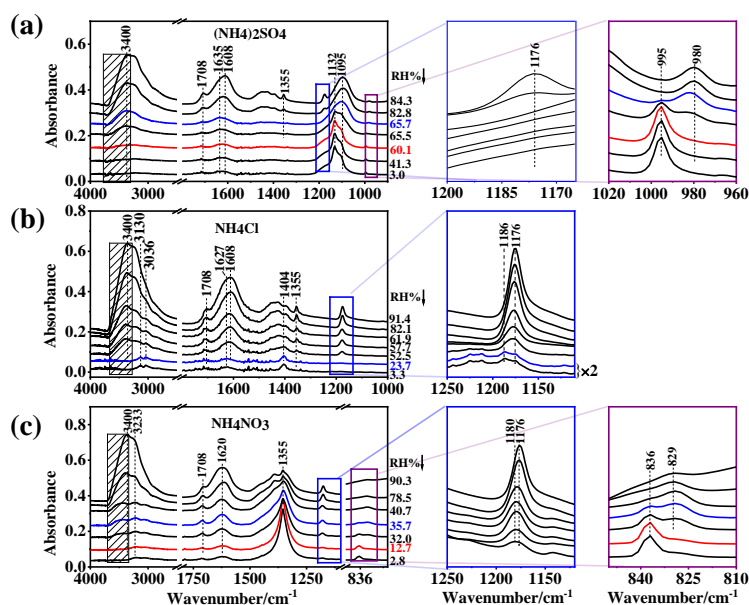
Figure 1: The FTIR spectra of mixed aerosols containing sodium pyruvate and various ammonium salts measured in this study and in previous work. (a) ammonium sulfate (Yang et al., 2019), (b) ammonium chloride, (c) ammonium nitrate on dehydration. The spectral data for sodium pyruvate and ammonium sulfate was previously reported by Yang et al (2019). The shaded area shows the chosen integration region for liquid water.
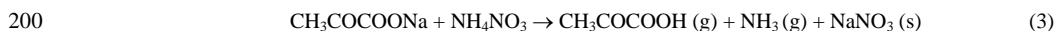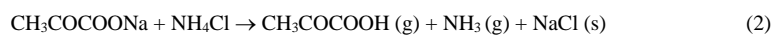
As the RH increased, the water content of the three SP/ammonium mixture systems increased, characterized by the bands at 3355/3400 cm^{-1} and 1640 cm^{-1} (Fig. S3 in the Supplement). The characteristic bands of SP became negligible, indicating trace or no SP remaining in aerosols. While for SP/$(NH_4)_2SO_4$ aerosols, only the 995 cm^{-1} band was found below 88.8% RH, indicating solid Na_2SO_4 without liquid SO_4^{2-} in the particles. From 88.8% RH, two bands are present at 980 cm^{-1} and 995 cm^{-1}, indicating the coexistence of liquid SO_4^{2-} and solid Na_2SO_4. As the RH continues to rise, the 995 cm^{-1} band decreased rapidly, and then almost vanished at 95.2% RH, suggesting the deliquescence of aerosols. In the IR spectra of SP/NH_4Cl aerosols, the bands from solid NH_4^+, i.e. 3130 cm^{-1}, 3036 cm^{-1} and 1404 cm^{-1} decreased gradually and disappeared at 71.8% RH, indicating the depletion of ammonium during hydration. In the IR spectra of SP/NH_4NO_3 particles, the band at 829 cm^{-1} begins to appear at 76.5%, indicating the dissolution of $NaNO_3$ solid. When the RH reached 81.9%, the band at 836 cm^{-1} disappeared, suggesting complete deliquescence of $NaNO_3$.

3.3 The replacement reaction in organic/ammonium aerosols

Based on the IR features observed, the following reactions (1) - (3) should have occurred:

$$CH_3COCOONa + (NH_4)_2SO_4 \rightarrow CH_3COCOOH\,(g) + NH_3\,(g) + Na_2SO_4\,(s) \qquad (1)$$

$$CH_3COCOONa + NH_4Cl \rightarrow CH_3COCOOH\,(g) + NH_3\,(g) + NaCl\,(s) \qquad (2)$$

200

$$CH_3COCOONa + NH_4NO_3 \rightarrow CH_3COCOOH\,(g) + NH_3\,(g) + NaNO_3\,(s) \qquad (3)$$

In systems containing sodium pyruvate, pyruvic acid and ammonia are formed and depleted from particles alongside the solid formation of various inorganic salts during dehydration. In bulk solution, it is well established that solid compound formation and gas evaporation can drive chemical reactions. Wang et al. (2017) observed the formation of lower hygroscopic ammonium hydrogen oxalate ($NH_4HC_2O_4$) and ammonium hydrogen sulfate

205 (NH_4HSO_4) from interactions between oxalic acid and ammonium sulfate in aerosols during the dehydration process. Herein, aerosol particles act as micro-reactors, with their larger specific surface area facilitating similar processes. In fact, both solid formation and the evaporation of gaseous compounds within particles can induce chemical reactions. Building upon previous findings regarding the formation of solid Na_2SO_4 from $(CH_2)_n(COONa)_2$ (n = 1, 2)/$(NH_4)_2SO_4$ aerosols upon dehydration, solid $NaNO_3$ and $NaCl$ are also formed, as

210 shown in equations (2) and (3) (Wang et al. 2019).

The phase state of aerosol particles strongly depends on their water content, which in turn is influenced by changes in ambient RH (Yeung et al., 2010). Conventionally, soluble inorganic aerosol particles spontaneously absorb water to form solution droplets upon hydration, and these droplets recrystallize upon dehydration. Pure inorganic particles, such as $NaCl$ and $(NH_4)_2SO_4$, often undergo prompt phase transitions reflected by sudden

215 water loss or uptake. Conversely, pure organic aerosols exhibit more diverse hygroscopic behaviors, forming either (poly)crystalline states or semisolids (Kuang et al., 2010). When mixtures of compounds are present in aerosols, as is ubiquitous in atmospheric aerosols and in $PM_{2.5}$, phase transitions may occur for all components or only a portion of them. Even if all constituents effloresce, the critical RH values vary compared to pure compounds. Consequently, the water content may not be indicative of the efflorescence or deliquescence process. For aerosols

220 composed of sodium pyruvate and ammonium, the response of water content to ambient RH is dependent upon water vapor equilibrium, replacement reaction, product depletion, and phase transitions. These processes result in sudden changes in water content that are inconsistent with spectral changes that are associated with phase transitions.

In Fig. 2, a significant deviation between the RH at which phase changes occur and the RH at which water

225 content changes abruptly can be observed. We note that the SP/$(NH_4)_2SO_4$ data was previously reported in Yang et al (2019). The sensitive RH range for SP/$(NH_4)_2SO_4$, where abrupt water loss occurs, ranged from 66.5 to 59.8% RH, overlapping with the phase change RH (red frame) during dehydration. Conversely, the deliquescence

9

range of Na$_2$SO$_4$ (pink frame) occurs at higher RH values than the abrupt water absorption range of 74.4-87.3%

RH during hydration. In the case of SP/NH$_4$Cl, the coexistence of aqueous and solid SP (red frame) occurs at RH

230   values much lower than the range of sudden water loss (61.7-42.2% RH). When the RH indreases, obvious water

uptake takes place from 68.9% RH to 80.9% RH. In previous studies, NH$_4$NO$_3$ was often believed to form a

viscous gel, leading to gradual dehydration with decreasing RH (Li et al., 2017). However, the produced NaNO$_3$

undergoes an aqueous-to-solid transformation within the RH range of 35.7%-12.7%, while maintaining almost

constant water content. During hydration, excessive water absorption occurs in the range of 72.7%-82.1% RH,
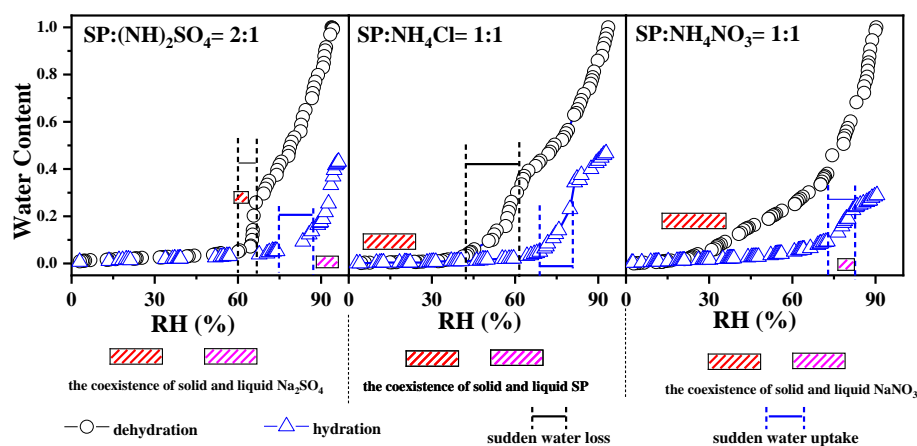
235   covering the deliquescence RH of NaNO$_3$.

Figure 2: Hygroscopicity curve of (a) SP: (NH$_4$)$_2$SO$_4$ =2:1 aerosols, (b) SP: NH$_4$Cl =1:1 aerosols and (c) SP: NH$_4$NO$_3$ =1:1 aerosols. The data for aerosols with SP: (NH$_4$)$_2$SO$_4$ =2:1 was previously reported by Yang et al (2019). The stoichiometric ratio between SP and (NH$_4$)$_2$SO$_4$ was set to 2:1 to keep the equivalent amount of organics and ammonium. In comparison, SP/NH$_4$Cl aerosols and SP/NH$_4$NO$_3$ aerosols also have equivalent amount of organics and ammonium.

240

3.4 The effect of organics on phase transition point

When inorganic compounds are mixed with organics, the efflorescence and deliquescence points are modified due

to intermolecular interactions. For instance, organic acids have been found to influence the phase transitions and

water uptake of ammonium sulfate (AS) aerosols (Shi et al., 2017). Similarly, organic salts can enhance water

245   uptake, sometimes reaching levels comparable to those of typical inorganic salts such as NaCl and (NH$_4$)$_2$SO$_4$.

Wu et al. (2011) observed a clear shift in the deliquescence relative humidity (DRH) of AS towards lower RH

values for mixtures of AS with organic acid salts, resulting in enhanced water uptake relative to mixtures with

organic acids alone. Additionally, Schroeder and Beyer (2016) noted that the onset DRH of organic salt/AS

mixtures was consistently lower than that of the pure components, irrespective of the fraction of organic salts in

250   the mixture.

Fig. 3 illustrates the RH ranges of efflorescence and deliquescence for comparison. It demonstrates the lower

efflorescence relative humidity (ERH) of Na_2SO_4, $NaNO_3$, and SP in mixtures compared to those in pure aerosols,

indicating that the presence of organics in the mixed particles can inhibit the crystallization of the produced

inorganics. In contrast to crystallization, the DRH of Na_2SO_4 and $NaNO_3$ in mixtures were slightly higher than

255   those of pure aerosols with a narrower DRH range. This deviates from previous experimental measurements and

thermodynamic model predictions, which suggested a significant reduction in aerosol DRH due to the mixing of

organic acids and inorganic salts (Bouzidi et al., 2020; Hodas et al., 2015).
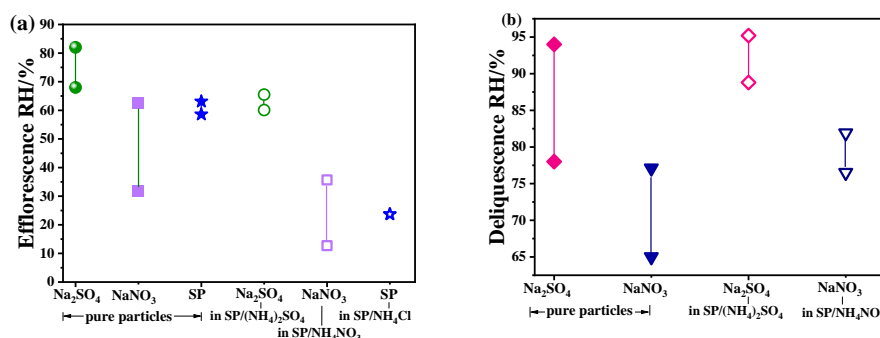
Figure 3: The efflorescence RH (a) and deliquescence RH (b) for single component aerosols (pure particles) and
260   **SP/ammonium particles.**

3.5 The effect of molar ratio to the replacement reaction and phase transition

The chemical reactivity and phase state of aerosols are often influenced by individual compounds within internally

mixed particles. In this study, SP/NH_4Cl particles were selected as a surrogate to investigate the dependence of

component reconstruction and phase transition on the molar ratio of SP to NH_4Cl. Mixture SP/NH_4Cl aerosols

265   were prepared with molar ratios of 1:2, 1:1, and 2:1. Fig. S4 presents the IR spectra in the range of 4000-800 cm$^-$

^{1} for 2:1, 1:1, and 1:2 SP/NH_4Cl ratios. When the molar ratio of SP to NH_4Cl was 2:1, the band changes were

reversible during dehydration and hydration cycle, with the absence of the 3130 cm^{-1} band. The band shift between

1608 cm^{-1} and 1627 cm^{-1} indicated the transition of SP between the liquid and solid phases.

For 1:1 SP/NH_4Cl particles, the IR spectra were shown in Fig.1(b) and Fig. S3(b) and described above. In

270   the case of 1:2 SP/NH_4Cl aerosols, the band at 3130 cm^{-1} was observed at 55.1% RH during dehumidification and

disappeared at 77.7% RH during humidification. Following a dehumidification-humidification cycle, the overall

quantity of compounds within the aerosol particles decreased, as reflected by the lower IR band intensity.

Fig. S5 displayed the IR spectra in the range of 1220-1120 cm^{-1} during dehydration, providing detailed band

shift and intensity information of the 1176 cm^{-1} band. Additionally, the quantified peak position and integrated

275   peak areas of SP/NH$_4$Cl particles, which can characterize the phase state and degree of chemical reaction, were

depicted in Fig. 4. The band at 1176 cm^{-1} indicates that the aerosols are in the aqueous phase, while its shift to

1186 cm^{-1} signifies the transition to solid-phase particles. Thus, the onset of efflorescence relative humidity (ERH)

can be identified by the appearance of the 1186 cm^{-1} peak. From Fig. 4(a), the onsets of ERH were approximately

41% and 23.7% for 2:1 and 1:1 SP/NH$_4$Cl particles, respectively. However, for NH$_4$Cl-rich mixtures, the band at

280   1182 cm^{-1} rather than 1186 cm^{-1} was observed at the lowest RH of 4.2%, indicating the formation of SP semisolids

due to the uptake of trace amounts of moisture. This suggests that the presence of NH$_4$Cl hindered the

crystallization of SP.

The integrated absorbance spanning from 1220 cm^{-1} to 1120 cm^{-1} demonstrates the evolution of SP content

during dehumidification in Fig. 4(b). The data indicate values of approximately 0.56, 0.06, and 0.22 for 2:1, 1:1,

285   and 1:2 SP/NH$_4$Cl mixtures, respectively, when the RH reached its minimum value. This implies that the degree

of reaction was maximum when SP was mixed with NH$_4$Cl in equal moles, lending credence to the reaction
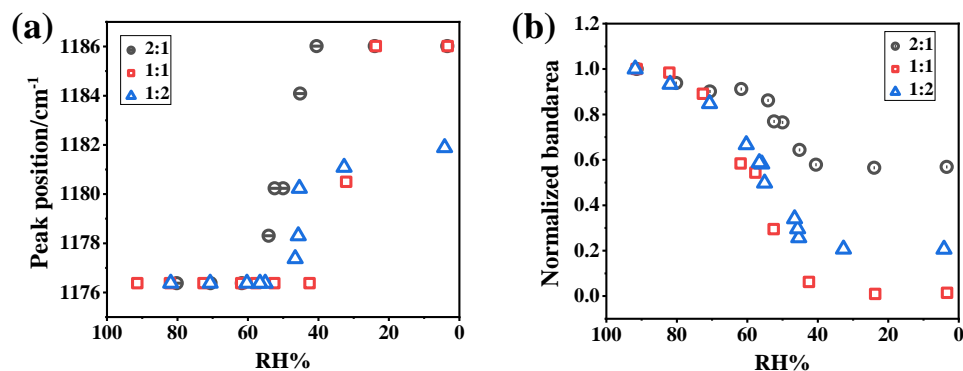
mechanism proposed by Wang et al. in 2019.

Figure 4: (a) The peak position shift from 1176 to 1186 cm^{-1} and (b) the integrated areas corresponding integrated
290   **band-area for 2:1, 1:1 and 1:2 SP/NH$_4$Cl particles during the dehumidification.**

3.6 The impact of replacement reaction on organic/ammonium sulfate aerosol phase state

The component evolution and aerosol phase transition are dependent upon multi processes containing

intermolecular interaction, ion mobility, gas-particle partitioning, ion-pair formation, replacement reaction and

dissociation et al., which originated from the composition of the internally mixed aerosols (Li et al., 2021;

295   Mikhailov et al., 2004). In this section, various organic salts, mixing with $(NH_4)_2SO_4$ was measured to explore the

phase behaviors of atmospheric sulfate aerosols. Unlike SP, the applied sodium citrate (SC) and sodium tartrate

(ST) exhibit viscous state at lower RH without DRH and ERH.

          Fig. 5 displays the IR spectra of SC/$(NH_4)_2SO_4$ and ST/$(NH_4)_2SO_4$ particles on dehydration. In Fig. 5(a), as

the RH decreases, the bands at 1575 cm^{-1} and 1391 cm^{-1} decreased whereas the 1715 cm^{-1} peak gradually increased,

300   which indicates decrease of the -COO$^-$ and the increase of -COOH. Other observations include the degenerated

band at 1095 cm^{-1}. When the RH decreases to 56.9%, the band at 1132 cm^{-1} appeared, as well as the band at 995

cm^{-1} for crystallized sulfate, indicating the solid Na_2SO_4 formation. As the RH further decreased, the 995 cm^{-1}

band for crystalline sulfate escalated, accompanying the weaker 980 cm^{-1} absorption peak, suggesting a growing

solid Na_2SO_4 content in the particles. While for ST/$(NH_4)_2SO_4$ mixture in Fig. 5(b), we observed the increasing

305   band at 1715 cm^{-1} and the replacement of 1587 cm^{-1} band by the 1597 cm^{-1} band, indicating the transformation

from sodium tartrate to sodium bitartrate. In addition, no solid formed in the aerosols since neither 1132 cm^{-1} nor

996 cm^{-1} was observed during the whole dehydration process.

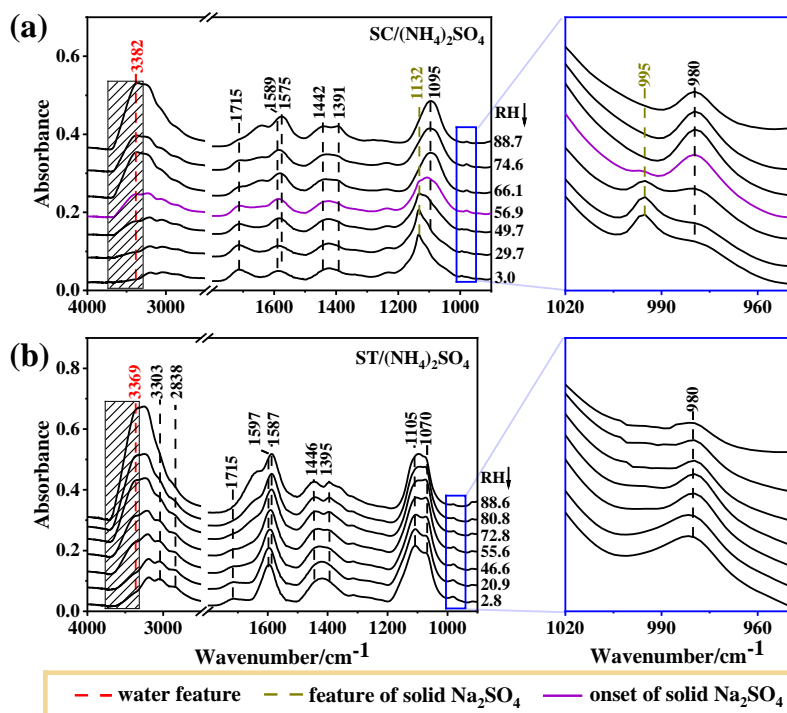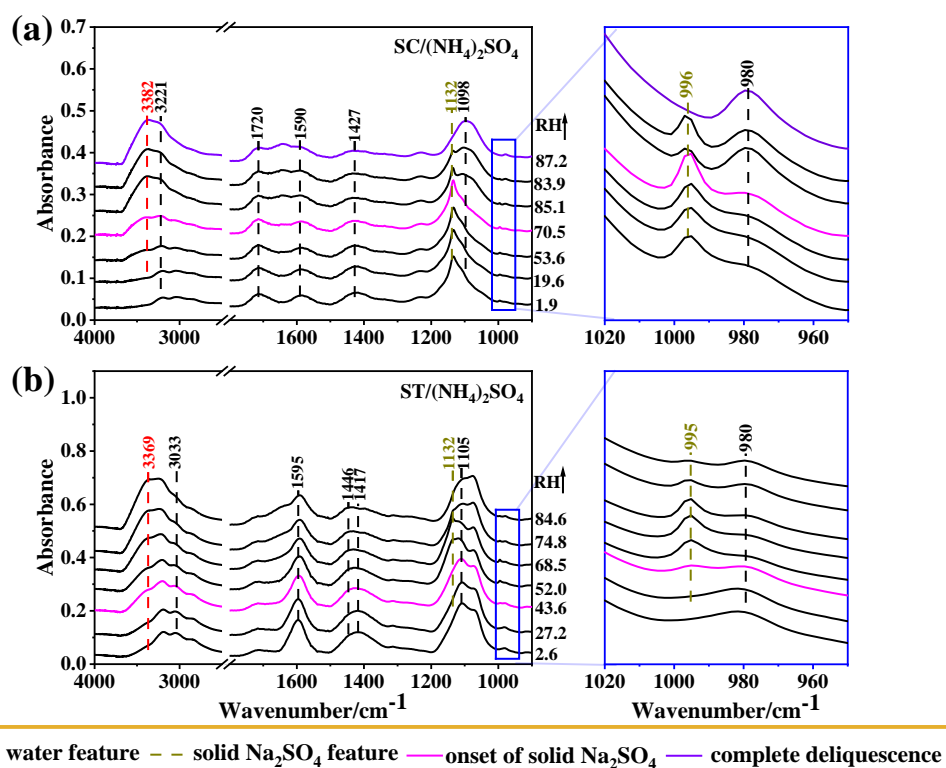Figure 5: The FTIR spectra of (a) 2:3 SC/$(NH_4)_2SO_4$ and (b) 1:1 ST/$(NH_4)_2SO_4$ aerosols on dehydration.

Fig. 6(a) shows the IR spectra as a function of RH for SC/(NH$_4$)$_2$SO$_4$ during the hydration process. As the

RH increases, the band at 1132 cm^{-1} maintains a constant intensity below 70.5% RH with a slight enhancement of

water features. At 70.5% RH, the band at 1132 cm^{-1} weakens with a notable increase in the 980 cm^{-1} band,

indicating the onset of Na$_2$SO$_4$ dissolution. The aerosol, mainly consisting of Na$_2$SO$_4$, completely deliquesces at

87.2% RH as the band at 996 cm^{-1} disappears entirely.

Figure 6: The FTIR spectra of (a) 2:3 SC/(NH$_4$)$_2$SO$_4$ and (b) 1:1 ST/(NH$_4$)$_2$SO$_4$ aerosols on hydration.

The IR spectra of ST/(NH$_4$)$_2$SO$_4$ particles are depicted in Fig. 6(b). Upon hydration, bands at 1132 cm^{-1} and

995 cm^{-1} are observed at 43.6% RH, suggesting an unexpected formation of solid Na$_2$SO$_4$. As the RH further

increases, the IR features of solid Na$_2$SO$_4$ weaken, almost disappears at 84.6% RH, indicating the deliquescence

of Na$_2$SO$_4$. Similar unconventional behavior of "crystallization on hydration" was also observed for mixed

gluconic acid/(NH$_4$)$_2$SO$_4$ and gluconic acid/NaCl aerosols using optical images, where solid (NH$_4$)$_2$SO$_4$ and NaCl

formed upon hydration (Zhu et al., 2022). Likewise, optical images of ST/(NH$_4$)$_2$SO$_4$ were monitored to verify

the phase and morphologies during an RH cycle. As shown in Fig. 7, the particle shape remains round and smooth,

14

indicative of a homogeneous aqueous state during dehydration, with a shrinking volume as RH increases. During

325   humidification, the particles maintain a uniform state with a round shape below 44% RH. At 44% RH, some

apparent rectangular dark entities, indicating solid formation, can be observed within the round particles.

Combining the above IR features and morphologies, the aerosols at 44% RH consist of solid Na_2SO_4, aqueous

$(NH_4)_2SO_4$, and SC. When the RH increases to 80.3% RH, the round and bright sphere is restored, indicating

aerosol deliquescence.

dehydration   hydration

| **94.1%RH** | **70.1%RH** | **12.1%RH** | **29.0%RH** | **44.0%RH** | **80.3%RH** |
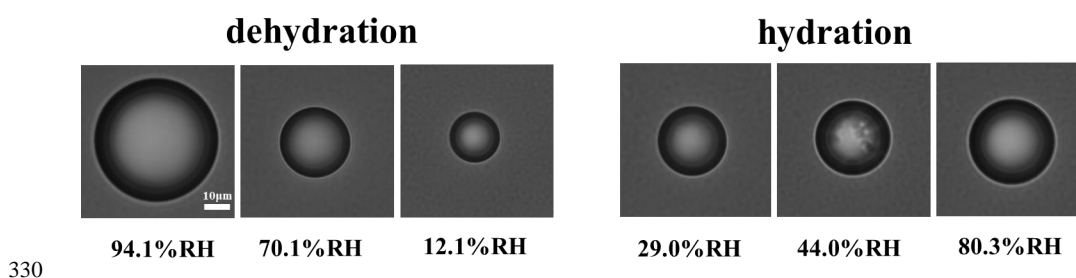
330

Figure 7: The optical morphologies of 1:1 ST/(NH₄)₂SO₄ aerosols during a down-up RH cycle.

As shown in Fig. 5 and Fig. 6, the IR spectra of SO_4^{2-} and organic salts remained distinguishable, indicating

incomplete reaction likely due to mass transfer limitations in viscous aerosol particles. With higher viscosity, the

degree of chemical reaction tends to decrease. Considering the correlation between the degree of replacement

335   reaction and water content, if the reaction remains incomplete after a RH cycle, the water content in the solution

state during hydration is lower than that during dehydration (Li et al., 2017). The gaps in water content between

dehydration and hydration during two RH cycles are illustrated in Fig. S6. For SP/(NH₄)₂SO₄ aerosols, full

recovery of water was observed after the second RH cycle, indicative of complete reaction and mainly Na_2SO_4

presence in the particles, consistent with the absence of IR absorptions from $(NH_4)_2SO_4$ and SP in Fig. S3(a).

340   However, for SC/(NH₄)₂SO₄ and ST/(NH₄)₂SO₄ mixed aerosols, the normal water absorption decreased by 0.1

and 0.14, respectively, after a second RH cycle, providing evidence of the viscous state of the mixed aerosols.

3.7 The Na₂SO₄ efflorescence upon hydration induced by the replacement reaction

Pöhlker et al. (2014) applied X-ray microspectroscopy to internally mixed aerosol particles from the Amazonian

rainforest collected during anthropogenic pollution and found changes in particle microstructure upon hydration,

345   primarily driven by efflorescence and recrystallization of sulfate salts during aerosol hydration. The efflorescence

upon hydration was attributed to aerosol viscosity and surface tension. Upon hydration, the initially amorphous

state of particles is in a metastable state where the formation of the solid phase is thermodynamically favored but kinetically hindered by nucleation. Continuous water uptake by the particles with rising RH is accompanied by decreasing aerosol viscosity and increasing ion mobility, which could overcome the kinetic inhibition of ion

350   movement at a certain RH level, leading to nucleation and crystal growth. However, the molecular structure was unknown in Pöhlker's study. Notwithstanding the viscous state for most organics, efflorescence upon hydration is rare. In fact, previous substantial work on the phase state evolution of internally mixed organic/inorganic particles showed ordinary efflorescence upon dehydration, and to the best of our knowledge, no similar crystallization upon humidification has been reported besides Pöhlker's study. In this work, SC particles retained viscous state at lower

355   RH levels as addressed above, while Na_2SO_4 crystallized upon dehydration from $SC/(NH_4)_2SO_4$ particles. Therefore, the effect of the molecular structure of organics on inorganic efflorescence needs to be further explored.

       According to our recent study on mixture aerosols of gluconic acid and $(NH_4)_2SO_4$ or NaCl, and the Na_2SO_4 crystallization from ST and $(NH_4)_2SO_4$ mixtures observed herein, we found that polyhydroxy acids or organic salts containing full-hydroxyl carbon chains is likely causing the efflorescence upon dehydration owing to more

360   viscosity. Grayson et al has demonstrated viscosity increasing as the number of hydroxyl groups in the molecule (Grayson et al., 2017). As the RH decreased, the polyhydroxy chain with a carboxyl group is prone to form a gel owing to intermolecular hydrogen bonding. When ST was mixed with $(NH_4)_2SO_4$, the polyhydroxy skeleton remained unchanged, and a gel structure gradually formed with the decrease in RH. Based on the fact of the gel state of internally mixed $ST/(NH_4)_2SO_4$ particles, the mechanism for efflorescence upon hydration was proposed

365   (shown in Fig. 8). During the first RH cycle, the ions can transfer freely in the aqueous aerosol. As the RH decreased, tartrate ions and acidified hydrogen tartrate self-assembled into aggregates and gradually gelatinized water due to a decrease in water content. Gels are two-phase mixtures of liquids dispersed in (semi-)solid amorphous matrices, and the uptake of water into a gel can involve gradual swelling as well as stepwise volume increases related to thermodynamically well-defined phase transitions. Upon drying, gels can form highly porous

370   structures (Li and Gong, 2024; Pang et al., 2002; Díaz-Marín et al., 2022). Therefore, in the gel structure, there may exist a collection of fine fibers in these gels which mechanical entanglements create a three-dimensional supramolecular structure to trap water molecules (Fig. 8). Due to the strong interaction between OH groups and SO_4^{2-} ions, anions were bound around fibers and migration was inhibited so that SO_4^{2-} and Na^+ ions cannot contact and nucleate. The gel structure is a metastable state with a higher energy state than the crystalline state. Upon

375   hydration following dehydration, the initial metastable aerosol can overcome the energy barrier to restore ion mobility in the particle; in turn, the anions and cations can combine to further form a solid nucleus. Continuously

elevating RH provided more water content in particles, inducing crystal formation from the metastable state

surrounded by a more stable solution employed gradually. Further water uptake can overcome the lattice energy

to perform a solid-to-aqueous phase transition, resulting in complete dissolution of solid Na_2SO_4 and aerosol
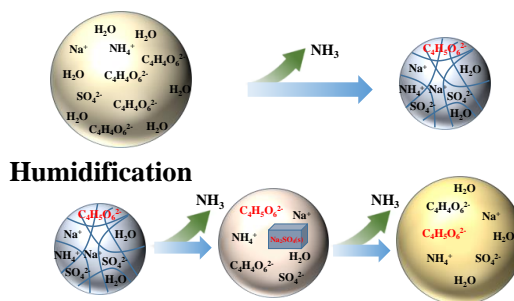
380   deliquescence.

Dehumidification

Humidification

Figure 8: the schematic phase behavior and chemical process of 1:1 ST/$(NH_4)_2SO_4$ particles on dehumidification and humidification.

4 Conclusions

385   Our findings illustrate that the aqueous replacement reaction within internally mixed organic/ammonium aerosols

can alter the aerosol composition which in turn affects the phase behavior of aerosol particles. As carboxylic acids

and carboxylate salts are abundant in the internal mixtures of atmospheric secondary aerosols (Huang et al., 2022),

our result implies that the aqueous phase reactions are significant process that can potentially dictate and

complicate the phase behavior of internally mixed organic/inorganic aerosols. The change of ERH and DRH, and

390   the occurrence of efflorescence upon humidification, due to the replacement reaction in organic/ammonium

aerosols, is crucial for the interaction between aerosols, water vapor, and trace gases, and potentially cause

uncertainty for the prediction of atmospheric aerosol phase state. Through the analysis of ATR-FTIR spectra from

multiple organic/ammonium aerosol systems under RH cycling, we have provided valuable insights into the

complex interactions between organic and inorganic components within aerosol particles.

395   By examining the hygroscopic behavior and phase transitions of internally mixed particles containing

organic acid salts and ammonium salts, we have uncovered the occurrence of replacement reactions and aerosol

component depletion during RH changes. Additionally, we observed unconventional crystallization upon

hydration behavior for the organic/ammonium mixture aerosols. The phase states of aerosols, including crystalline,

aqueous, and gel-like states during dehydration and hydration cycles, provide insights into a deeper understanding

400   of the factors influencing aerosol hygroscopicity and phase behavior.

Our findings highlight the intricate interplay between chemical components of organic/inorganic aerosol, such as organic molecular structure, viscosity, replacement reaction and their collective impact on aerosol phase state. The observed variations in replacement reactions and product depletion, as well as phase transitions, emphasizes the complexity of aqueous phase aerosol chemistry and its impact on atmospheric processes.

405   Furthermore, the identification of molecular structure-dependent effects on aerosol phase state provides valuable information for developing targeted strategies to mitigate air pollution and its associated impacts on climate and public health. By considering the diverse compositions and phase behaviors of internally mixed organic/inorganic aerosol, we can better understand and address the challenges posed by air pollution remediation and climate change.
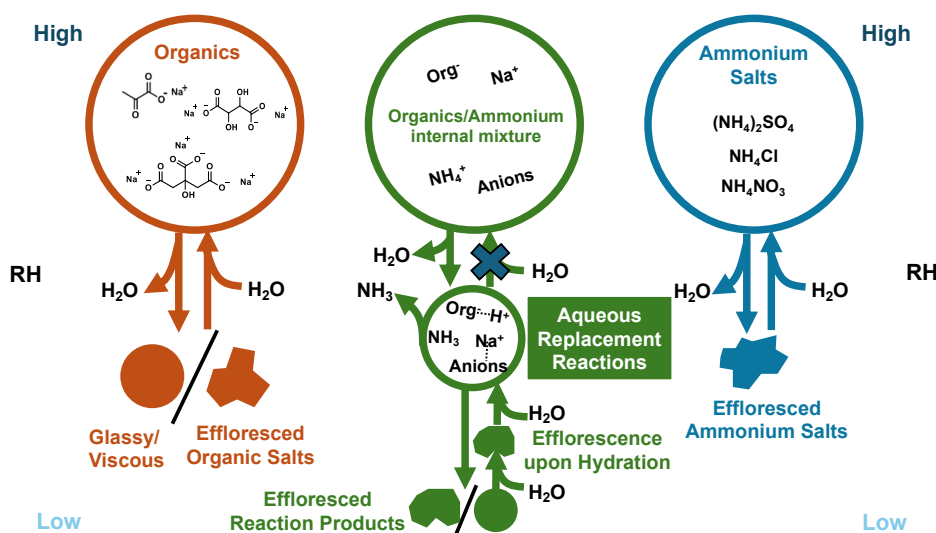
410

Figure 9: the schematic of the impact of aqueous replacement reactions on the phase behavior of internally-mixed organic/inorganic aerosols.

Data availability

Data is available upon request by contacting the corresponding authors.

415   **Supplement**

The supporting information includes further experimental details and supplementary figures that are associate with the main text.

Author contributions

420 S.P. conceptualized, designed the study. Y.Z., S.P. supervised the study. H.Y., F.D., L.X., conducted the expeirments. H.Y., S.P. analyzed and visualized the data, and worte the orginal draft. Q.H., S.P. reviewed and edited the manuscript.

Competing interests.

The authors declare that they have no conflict of interest.

References

Bouzidi, H., Zuend, A.; Ondráèek, J., Schwarz, J. and Ždímal, V.: Hygroscopic behavior of inorganic–organic

430 aerosol systems including ammonium sulfate, dicarboxylic acids, and oligomer, Atmos. Environ., 229, 117481, https://doi.org/10.1016/j.atmosenv.2020.117481, 2020.

Chen, Z., Liu, P., Liu, Y., Zhang, Y.: Strong Acids or Bases Displaced by Weak Acids or Bases in Aerosols: Reactions Driven by the Continuous Partitioning of Volatile Products into the Gas Phase, Acc. Chem. Res., 54, 3667−3678, https://doi.org/10.1021/acs.accounts.1c00318, 2021.

435 Chen, Z., Liu, P., SU, H., Zhang, Y.: Displacement of Strong Acids or Bases by Weak Acids or Bases in Aerosols: Thermodynamics and Kinetics, Environ. Sci. Technol., 56, 12937−12944, https://doi.org/10.1021/acs.est.2c03719, 2022.

Díaz-Marín, C. D., Zhang, L., Lu, Z., Alshrah, M., Grossman, J. C., Wang, E. N.: Kinetics of Sorption in Hygroscopic Hydrogels, Nano Lett., 22, 1100−1107, https://doi.org/10.1021/acs.nanolett.1c04216, 2022.

440 Du, C., Wang, W., Wang, N., Pang, S., Zhang, Y.: Impact of ambient relative humidity and acidity on chemical composition evolution for malonic acid/calcium nitrate mixed particles, Chemosphere, 276, 130140, https://doi.org/10.1016/j.chemosphere.2021.130140, 2021.

Du, C., Yang, H., Wang, N., Pang, S., Zhang, Y.: pH effect on the release of NH3 from the internally mixed sodium succinate and ammonium sulfate aerosols, Atmos. Environ. 220, 11710,

445   https://doi.org/10.1016/j.atmosenv.2019.117101, 2020.

Furukawa, T., Takahashi, Y.: Oxalate metal complexes in aerosol particles: implications for the hygroscopicity of oxalate-containing particles, Atmos. Chem. Phys., 11, 4289−4301, https://doi.org/10.5194/acp-11-4289-2011, 2011.

Freedman, M. A., Huang, Q., Pitta, K. R.: Phase Transitions in Organic and Organic/Inorganic Aerosol Particles,
450   Annu. Rev. Phys. Chem., https://doi.org/10.1146/annurev-physchem-083122-115909, 2024.

Grayson, J. W., Evoy, E., Song, M., Chu, Y., Maclean, A., Nguyen, A., Upshur, M. A., Ebrahimi, M., Chan, C. K., Geiger, F. M., Thomson, R. J., Bertram, A. K.: The effect of hydroxyl functional groups and molar mass on the viscosity of non-crystalline organic and organic–water particles, Atmos. Chem. Phys., 17, 8509–8524, https://doi.org/10.5194/acp-17-8509-2017, 2017.

455 Hodas, N., Zuend, A.; Mui, W., Flagan, R. C., Seinfeld, J. H.: Influence of particle-phase state on the hygroscopic behavior of mixed organic–inorganic aerosols, Atmos. Chem. Phys., 15,5027–5045, https://doi.org/10.5194/acp-15-5027-2015, 2015.

Huang, S., Wu, Z., Wang, Y., Poulain, L., Höpner, F., Merkel, M., Herrmann, H., Wiedensohler, A.: Aerosol Hygroscopicity and its Link to Chemical Composition in a Remote Marine Environment Based on Three
460   Transatlantic Measurements, Environ. Sci. Technol., 56, 9613−9622, https://doi.org/10.5194/acp-2019-839, 2022.

Jia, X., Gu, W., Peng, C., Li, R., Chen, L., Wang, H., Wang, H., Wang, X., Tang, M.: Heterogeneous Reaction of $CaCO_3$ With NO_2 at Different Relative Humidities: Kinetics, Mechanisms, and Impacts on Aerosol Hygroscopicity, J. Geophys. Res.: Atmos. 126, e2021JD034826, https://doi.org/10.1029/2021JD034826,
465   2021.

Jing, B., Tong, S. R., Liu, Q. F., Li, K., Wang, W. G., Zhang, Y. H., Ge, M. F.: Hygroscopic behavior of multicomponent organic aerosols and their internal mixtures with ammonium sulfate, Atmos. Chem. Phys., 16, 4101−4118, https://doi.org/10.5194/acp-16-4101-2016, 2016.

Koop, T., Bookhold, J., Shiraiwa, M., and Poschl, U.: Glass Transition and Phase State of Organic Compounds:
470   Dependency on Molecular Properties and Implications for Secondary Organic Aerosols in the Atmosphere, Phys. Chem. Chem. Phys., 13, 19238–19255, https://doi.org/10.1039/C1CP22617G, 2001.

Kreidenweis, S. M., Koehler, K., DeMott, P. J., Prenni, A. J., Carrico, C., Ervens, B.: Water Activity and Activation Diameters from Hygroscopicity Data—Part I: Theory and Application to Inorganic Salts, Atmos. Chem. Phys. 5, 1357–1370, https://doi.org/10.5194/acp-5-1357-2005, 2005.

475   Kuang, Y., Xu, W., Tao, J., Ma, N., Zhao C., Shao, M.: A Review on Laboratory Studies and Field Measurements
        of Atmospheric Organic Aerosol Hygroscopicity and Its Parameterization Based on Oxidation Levels, Curr.
        Poll. Rep., 6, 410–424, https://doi.org/10.1007/s40726-020-00164-2, 2010.

        Li, Q.; Ma, S.; Liu, Y.; Wu, X.; Fu, H.; Tu, X.; Yan, S.; Zhang, L.; George, C.; Chen, J. Phase State Regulates
        Photochemical HONO Production from NaNO$_3$/Dicarboxylic Acid Mixtures. Environ. Sci. Technol., 58,
480   7516-7528, https://doi.org/10.1021/acs.est.3c10980, 2024.

        Li X., Gong, J. P.: Design principles for strong and tough hydrogels, Nat. Rev. Mater.,
        https://doi.org/10.1038/s41578-024-00672-3, 2024.

        Li, X., Gupta, D., Lee, J., Park, G., Ro, C.U.: Real-time investigation of chemical compositions and hygroscopic
        properties of aerosols generated from NaCl and malonic acid mixture solutions using in situ Raman
485   microspectrometry, Environ. Sci. Technol., 51, 263–270, https://doi.org/10.1021/acs.est.6b04356, 2017.

        Li, X., Wu, L., Lee J.-S., Ro, C.-U.: Hygroscopic behavior and chemical reactivity of aerosols generated from
        mixture solutions of low molecular weight dicarboxylic acids and NaCl, Phys. Chem. Chem. Phys., 23,
        11052-11064, https://doi.org/10.1039/d1cp00590a, 2021.

        Li, Y.-J., Liu, P.-F., Bergoend, C., Bateman A. P., Martin, S. T.: Rebounding hygroscopic inorganic aerosol
490   particles: Liquids,   gels,   and   hydrates,   Aero.   Sci.   Technol.,   51,   388-396,
        https://doi.org/10.1080/02786826.2016.1263384, 2017.

        Liu, P., Li, Y. J., Wang, Y., Gilles, M. K., Zaveri, R. A., Bertram, A. K., Martin, S. T.: Lability of Secondary
        Organic   Particulate   Matter,   Proc.   Natl.   Acad.   Sci.   USA,   113,   12643–12648,
        https://doi.org/10.1073/pnas.1603138113, 2016.

495   Liu, Y. J., Zhu, T., Zhao, D. F., Zhang, Z. F.: Investigation of the hygroscopic properties of Ca(NO$_3$)$_2$ and
        internally mixed Ca(NO$_3$)$_2$/CaCO$_3$ particles by micro-Raman spectrometry, Atmos. Chem. Phys., 8, 7205–
        7215, https://doi.org/10.5194/acpd-8-10597-2008, 2008.

        Ma, Q., Zhong, C., Liu, C., Liu, J., Ma, J., Wu, L., He, H.: A Comprehensive Study about the Hygroscopic
        Behavior of Mixtures of Oxalic Acid and Nitrate Salts: Implication for the Occurrence of Atmospheric
500   Metal Oxalate Complex, ACS Earth Space Chem., 3, 1216−1225,
        https://doi.org/10.1021/acsearthspacechem.9b00077, 2019.

        Ma, S., Li, Q., Zhang, Y.: A comprehensive study on hygroscopic behaviour and nitrate depletion of NaNO3 and
        dicarboxylic acid mixtures: implications for nitrate depletion in tropospheric aerosols, Atmos. Chem. Phys.,
        22, 10955–10970, https://doi.org/10.5194/acp-22-10955-2022, 2022.

505   Madawala, C. K., Lee, H. D., Kaluarachchi, C. P. and Tivanski, A. V.: Probing the Water Uptake and Phase State
        of Individual Sucrose Nanoparticles Using Atomic Force Microscopy, ACS Earth Space Chem., 5,
        2612−2620, https://doi.org/10.1021/acsearthspacechem.1c00101, 2021.

      Marcolli, C., Luo, B., Peter, T.: Mixing of the organic aerosol fractions: Liquids as the thermodynamically stable
        phases, J. Phys. Chem. A,108, 2216–2224, https://doi.org/10.1021/jp036080l, 2004.

510   Max, J.-J., Chapados, C.: Aqueous ammonia and ammonium chloride hydrates: principal infrared spectra. J. Mol.
        Struc., 1046,124–135, https://doi.org/10.1016/j.molstruc.2013.04.045, 2013.

      Mikhailov, E., Vlasenko, S., Martin, S. T., Koop, T., Pöschl, U.: Amorphous and crystalline aerosol particles
        interacting with water vapor: conceptual framework and experimental evidence for restructuring, phase
        transitions and kinetic limitations, Atmos. Chem. Phys., 9, 9491–9522, https://doi.org/10.5194/acp-9-9491-
515   2009, 2009.

      Mikhailov, E., Vlasenko, S., Niessner, R., Pöschl, U.: Interaction of aerosol particles composed of protein and
        salts with water vapor: hygroscopic growth and microstructural rearrangement, Atmos. Chem. Phys., 4,
        323–350, https://doi.org/10.5194/acp-4-323-2004, 2004.

      Miñambres, L., Méndez, E., Sánchez, M. N., Castaño, F., Basterretxea, F. J.: Water uptake of internally mixed
520   ammonium sulfate and dicarboxylic acid particles probed by infrared spectroscopy, Atmos. Environ., 70,
        108–116, http://dx.doi.org/10.1016/j.atmosenv.2013.01.007, 2013.

      Nemesure, S., Wagener, R., Schwartz, S. E.: Direct Shortwave Forcing of Climate by the Anthropogenic Sulfate
        Aerosol: Sensitivity to Particle Size, Composition, and Relative Humidity, J. Geophys. Res., 100, 26105–
        26116, https://doi.org/10.1029/95JD02897, 1995.

525   Pang, S., Zhu, D.: Pronounced hydrogel formation by the self-assembled aggregate of semifluorinated fatty acid,
        Chem. Phys. Lett., 358, 479−483, https://doi.org/10.1016/S0009-2614(02)00646-2, 2002.

      Peng, C. and Chan, C. K.: The water cycles of water-soluble organic salts of atmospheric importance, Atmos.
        Environ. 5, 1183–1192, https://doi.org/10.1016/s1352-2310(00)00426-x, 2001.

      Pilinis, C., Pandis, S. N., Seinfeld, J. H.: Sensitivity of Direct Climate Forcing by Atmospheric Aerosols to
530   Aerosols Size and Composition, J. Geophys. Res., 100, 18739–18754, https://doi.org/10.1029/95JD02119,
        1995.

      Pöhlker, C., Saturno, J., Krüger, M. L., Förster, J.-D., Weigand, M., Wiedemann, K. T., Bechtel, M., Artaxo,
        P. and Andreae, M. O.: Efflorescence upon humidification? X-ray microspectroscopic in situ
        observation of changes in aerosol microstructure and phase state upon hydration, Geophys. Res. Lett.,

535   41, 3681–3689, https://doi.org/10.1002/2014GL059409, 2014.

Prenni, A. J., DeMott, P. J., Kreidenweis, S. M.: Water uptake of internally mixed particles containing ammonium sulfate and dicarboxylic acids, Atmos. Environ. 37, 4243–4251, https://doi.org/10.1016/s1352-2310(03)00559-4, 2003.

Ren, H., Cai, C., Leng, C.-B., Pang, S.-F., Zhang, Y.-H.: Nucleation Kinetics in Mixed NaNO$_3$/Glycerol Droplets

540   Investigated with the FTIR−ATR Technique, J. Phys. Chem. B, 120, 2913−2920, https://doi.org /10.1021/acs.jpcb.5b12442, 2016.

Schroeder, J. R., Beyer, K. D.: Deliquescence relative humidities of organic and inorganic salts important in the atmosphere, J. Phys. Chem. A, 120, 9948−9957, https://doi.org/10.1021/acs.jpca.6b08725, 2016.

Shi, X. M., Wu, F. M., Jing, B., Wang, N., Xu, L. L., Pang, S. F., Zhang, Y. H.: Hygroscopicity of internally

545   mixed particles composed of (NH$_4$)$_2$SO$_4$ and citric acid under pulsed RH change, Chemosphere, 188, 532–540, https://doi.org/10.1016/j.chemosphere.2017.09.024, 2017.

Shi, Y., Ge, M., Wang, W.: Hygroscopicity of internally mixed aerosol particles containing benzoic acid and inorganic salts, Atmos. Environ., 60, 9−17, https://doi.org/10.1016/j.atmosenv.2012.06.034, 2012.

Shiraiwa, M., Pfrang, C., Koop, T., Poschl, U.: Kinetic Multi-Layer Model of Gas-Particle Interactions in Aerosols

550   and Clouds (KM-GAP): Linking Condensation, Evaporation and Chemical Reactions of Organics, Oxidants and Water, Atmos. Chem. Phys., 12, 2777–2794, https://doi.org/10.5194/acp-12-2777-2012, 2012.

Svenningsson, B., Hansson, H. C., Martinsson, B., Wiedensohler, A., Swietlicki, E., Cederfelt, S. I., Wendisch, M., Bower, K. N., Choularton, T. W., Colvile, R. N.: Cloud Droplet Nucleation Scavenging in Relation to the Size and Hygroscopic Behaviour of Aerosol Particles, Atmos. Envion., 31, 2463–2475,

555   https://doi.org/10.1016/S1352-2310(96)00179-3, 1997.

Tan, D.-T., Cai, C., Zhang, Y., Wang, N., Pang, S. –F., Zhang, Y. –H.: Crystallization kinetics from mixture Na$_2$SO$_4$/glycerol droplets of Na$_2$SO$_4$ by FTIR-ATR, Chem. Phys., 485, 131 –135, http://dx.doi.org/10.1016/j.chemphys.2016.07.007, 2014.

Wang, N., Cai, C., He, X., Pang, S.-F., Zhang, Y.-H.: Vacuum FTIR study on the hygroscopicity of magnesium

560   acetate aerosols, Spectrochim. Acta Part A: Mol. Bio. Spectrosc. 192, 420–426, https://doi.org/10.1016/j.saa.2017.11.058, 2018.

Wang, N., Jing, B., Wang, P., Wang, Z., Li, J., Pang, S., Zhang, Y., Ge, M.: Hygroscopicity and Compositional Evolution of Atmospheric Aerosols Containing Water-Soluble Carboxylic Acid Salts and Ammonium

Sulfate: Influence of Ammonium Depletion, Environ. Sci. Technol, 53, 6225−6234, https://doi.org/10.1021/acs.est.8b07052, 2019.

Wang, X., Jing, B., Tan, F., Ma, J., Zhang, Y., Ge, M.: Hygroscopic behavior and chemical composition evolution of internally mixed aerosols composed of oxalic acid and ammonium sulfate, Atmos. Chem. Phys., 17, 12797–12812, https://doi.org/10.5194/acp-17-12797-2017, 2017.

Wu, Z. J., Nowak, A., Poulain, L., Herrmann, H. and Wiedensohler, A.: Hygroscopic behavior of atmospherically relevant water-soluble carboxylic salts and their influence on the water uptake of ammonium sulfate, Atmos. Chem. Phys., 11, 12617–12626, https://doi.org/10.5194/acp-11-12617-2011, 2011.

Yang, H., Wang, N., Pang, S., Zheng, C., Zhang, Y.: Chemical reaction between sodium pyruvate and ammonium sulfate in aerosol particles and resultant sodium sulfate efflorescence, Chemosphere, 215, 554−562, https://doi.org/10.1016/j.chemosphere.2018.10.062, 2019.

Yeung, M. C., Chan, C. K.: Water Content and Phase Transitions in Particles of Inorganic and Organic Species and their Mixtures Using Micro-Raman Spectroscopy, Aero. Sci. Technol., 44, 269–280, https://doi.org/10.1080/02786820903583786, 2010.

Zardini, A. A., Sjogren, S., Marcolli, C., Krieger, U. K., Gysel, M., Weingartner, E., altensperger, U., Peter, T.: A combined particle trap/HTDMA hygroscopicity study of mixed inorganic/organic aerosol particles, Atmos. Chem. Phys., 8, 5589–5601, https://doi.org/10.5194/acp-8-5589-2008, 2008.

Zhang, Q. N., Zhang, Y., Cai, C., Guo, Y. C., Reid, J. P., Zhang, Y. H.: In situ observation on the dynamic process of evaporation and crystallization of sodium nitrate droplets on a ZnSe substrate by FTIR-ATR, J. Phys. Chem. A, 118, 2728−37, https://doi.org/10.1021/jp412073c, 2014.

Zhang, Z., Li, Y., Ran, H., An, J., Qu, Y., Zhou, W., Xu, W., Hu, W., Xie, H., Wang, Z., Sun, Y., Shiraiwa, M.: Simulated phase state and viscosity of secondary organic aerosols over China, Atmos. Chem. Phys., 24, 4809–4826, https://doi.org/10.5194/acp-24-4809-2024, 2024.

Zhu, Y., Pang, S., Zhang, Y.: Observations on the unique phase transitions of inorganics relevant due to gluconic acid in particles, Atmos. Environ., 288, 119313, https://doi.org/10.1016/j.atmosenv.2022.119313, 2022.

Zong, T., Wang, H., Wu, Z., Lu, K., Wang, Y., Zhu, Y., Shang, D., Fang, X., Huang, X., He, L., Ma, N., Größ, J., Huang, S., Guo, S., Zeng, L., Herrmann, H., Wiedensohler, A., Zhang, Y., Hu, M.: Particle hygroscopicity inhomogeneity and its impact on reactive uptake, Sci. Tot. Environ., 811, 151364, https://doi.org/10.1016/j.scitotenv.2021.151364, 2022.